

The pulsed soft X-ray emission from PSR 0656+14

A. Possenti

Dipartimento di Fisica, Università di Milano, via Celoria 16, I-20133 Milano, Italy

S. Mereghetti

Istituto di Fisica Cosmica del C.N.R., Via Bassini 15, I-20133 Milano, Italy

M. Colpi

Dipartimento di Fisica, Università di Milano, via Celoria 16, I-20133 Milano, Italy

Send offprint requests to: *S. Mereghetti; e-mail: sandro@ifctr.mi.cnr.it*

Accepted by Astronomy & Astrophysics on 29 February 1996

Abstract

We present the results of a spectral and timing analysis of PSR 0656+14 based on the complete set of ROSAT observations carried out with the PSPC instrument in 1991 and 1992. The present analysis confirms the thermal origin of the bulk of the emission in the soft X-ray band (Finley et al. 1992). In addition, we find strong evidence of a harder component, described equally well with a blackbody at $T \simeq 2 \times 10^6$ K, or with a steep power law with photon index $\Gamma \simeq 4.5$. This bimodal emission is also supported by an analysis of the light curve shape as a function of the energy.

The 0.1–2.4 keV light curve of PSR 0656+14, with a pulsed fraction of about 9%, is interpreted with a simple model for the temperature distribution on the neutron star surface, coupled with the geometrical information derived from radio data. In this model, which includes the effects of relativistic light bending and gravitational redshift, the X-rays originate from two thermal components resulting from neutron star cooling and blackbody emission released in the hotter polar cap regions.

The observed modulation can be reproduced only if PSR 0656+14 has a relatively high dipole inclination ($\sim 30^\circ$) and $(1+z) \lesssim 1.15$. The overall pulsed fraction cannot be significantly increased by including the polar cap contribution, if its temperature and intensity are to be consistent with the observed spectra.

1 Introduction

ROSAT observations of isolated neutron stars with characteristic ages of a few 10^5 years (PSR 0656+14, PSR 1055-52, Geminga) have shown that the bulk of their X-ray emission is thermal in origin and may result from neutron star cooling (see Ögelman 1995 for a review). The observed periodic modulation in the X-ray flux indicates the presence of large thermal gradients on the surface of these magnetized neutron stars. For a given surface temperature distribution, the degree of modulation depends on the intrinsic geometry of the source and

on its orientation relative to the observer, which in the case of radio pulsars can be inferred from the shape, polarization and spectrum of the radio pulses.

PSR 0656+14, first studied in the soft X-ray range with the Einstein Observatory (Cordova et al. 1989), is the brightest "middle-aged" neutron star in this energy band. Its association with a possible X-ray supernova remnant, the Gemini-Monoceros ring (Nousek et al. 1981; Thompson et al. 1991) has recently been criticized, on the basis of new results on the proper motion of the pulsar (Thompson & Cordova 1994). A candidate optical counterpart with $V \sim 25$ has been discovered by Caraveo, Bignami & Mereghetti (1994) within $1''$ of the radio position of PSR 0656+14.

Three pointings of PSR 0656+14 were carried out with the ROSAT PSPC detector (1991 March 26, 1992 March 24 and April 15). While the first observation (~ 3200 s) has been presented in detail by Finley, Ögelman & Kiziloğlu (1992), only the preliminary results of the two 1992 pointings have been reported (Ögelman 1995).

In this paper we analyze all the PSPC data of PSR 0656+14 and interpret them in the context of a simple model for its temperature distribution coupled with the geometrical configuration derived from the radio data. On the basis of the new observational results, the paper carries out an analysis similar to the one presented by Page (1995a) on PSR 0656+14 and explores the effect of polar cap emission on the light curves and spectra.

2 ROSAT observations: Data analysis and results

Our spectral analysis is based on the sum of the three observations, for a total exposure time of about 17000 s. The source counts were extracted from a circular region ($3'$ radius) centered at the position of PSR 0656+14. The background was estimated from a concentric annular region with radii $4'$ and $10'$ (due to the high source count rate of ~ 1.9 ct s^{-1} , the results are not significantly dependent on the particular region used for the background determination). The selected counts ($\sim 32,000$, in channels 11–240) were rebinned in order to achieve a minimum signal to noise ratio of 7 in each energy channel and then fitted to different model spectra.

Single component models (power law, blackbody, thermal bremsstrahlung) gave unacceptable results. Figure 1 shows the fit residuals obtained in the case of a blackbody (the model giving the lowest χ^2). While such a model was still compatible with the data of the first observation alone (Finley et al. 1992), the better statistics of the complete data set clearly require the presence of a second, harder component dominating the X-ray emission above ~ 1 keV. We therefore considered composite models, consisting of a "soft" blackbody and a "hard tail" in the form of either a second blackbody or a power law.

For the former case (see Figure 2a) a good fit ($\chi^2=1.07$ for 74 dof) was obtained with blackbody temperatures $T_1^\infty = 9.1 \times 10^5$ °K and $T_2^\infty = 1.9 \times 10^6$ °K for the soft and hard components, respectively, and an interstellar absorption $N_H = 6.9 \times 10^{19}$ cm $^{-2}$. Figure 3 (a,b) gives the confidence contours for these

quantities, while Table 1 summarizes the best fit values of all the parameters. The flux in the soft component implies an emitting region with radius $R^\infty \sim 14$ km (for a distance of 760 pc; Taylor et al. 1995). For the same distance, the total luminosity is about 10^{33} erg s^{-1} . Figure 2b shows the best fit with a blackbody plus power law, corresponding to a reduced $\chi^2=1.05$. The best fit photon index is $\Gamma = 4.5$. Contrary to the previous case, in this spectral decomposition both components have a similar flux. In the fit of the hard tail with a power law, one obtains values for N_H and for the soft blackbody temperature significantly higher than those of the two blackbody fit (see Figures 3c and 3d).

Table 1: Results of the spectral fit of PSR 0656+14

Model	N_H (10^{20}cm^{-2})	T^∞ ($10^6 \text{ }^\circ K$) or photon index Γ	Flux ($\text{erg cm}^{-2} \text{sec}^{-1}$)	R^∞ (km)	χ^2/dof
Blackbody (soft) +	0.7 ± 0.1	0.91 ± 0.05	1.3×10^{-11}	14.0	1.07
Blackbody (hard)		1.9 ± 0.4	9.4×10^{-13}	0.8	
Blackbody (soft) +	1.9 ± 0.4	1.01 ± 0.06	9.1×10^{-12}	9.1	1.05
Power-law		4.5 ± 0.4	4.1×10^{-11}	—	

Errors are at 90% confidence level for a single interesting parameter. R^∞ is for a distance $d=760$ pc. The fluxes are unabsorbed in the 0.1–2.4 keV range.

For the timing analysis, we only considered the two 1992 observations, since the relatively short time gap between them allows an accurate relative measure of the photon arrival times. In order to maximize the signal to noise ratio, the source counts were extracted from circles with different radii ($160'' - 50''$), matched to the PSPC point response function at the different energies. After the correction of the arrival times to the Solar System Barycenter, we folded the data using the P and \dot{P} values expected from the radio observations (Taylor et al. 1995), to obtain the 0.1 – 2.4 keV light curve shown in Figure 4 (we also verified that a standard period search resulted in a best value for P compatible with that expected from the radio data). The light curve shows a single broad peak, similar to that of the 1991 data (Finley et al. 1992), but with a slightly smaller pulsed fraction of $P_{fr} = 9\%$ ($P_{fr}=(CR_{ave}-CR_{min})/CR_{ave}$, where CR_{ave} and CR_{min} are the mean and minimum count rates). As shown in Figure 5, the degree of modulation and the phase of the peak depend on the photon energy: above ~ 0.5 keV the peak is narrower and shifted of about 70° . Contrary to the case of Geminga (Halpern & Ruderman 1993), there is no evidence of an anticorrelation between the pulsed fraction and the photon energy in the soft ($\lesssim 0.5$ keV) component (see also Page, Shibano & Zavlin 1995). The different shape and higher pulsed fraction above 0.5 keV in the light curves of PSR 0656+14, support the presence of two different components suggested by the spectral analysis.

3 Simulation of pulsed light curves

3.1 The model

Our model consists of the superposition of two contributions: a thermal component with nonuniform temperature distribution which arises from the whole surface, and an additional emission from hotter region(s) near the magnetic poles. The first component is modelled following the work by Greenstein & Hartke (1983), who derived the surface temperature gradient resulting from anisotropic heat transport from the hotter isothermal interior to the cooler surface. The degree of anisotropy of the heat flow, induced by a crustal magnetic field, is parameterized by the ratio of the coefficients of thermal conductivity orthogonal and parallel to the field: $K = k_{\perp}/k_{\parallel}$. In the hypothesis of a dipolar field, the surface temperature reaches a maximum at the magnetic poles (where the field is almost orthogonal to the surface) and a minimum along the magnetic equator. For middle aged neutron stars, such as PSR 0656+14, K is expected to lie in the range 0.0001 — 0.01 (Schaaf 1990; Hernquist 1985). Since the temperature distribution depends only weakly on K , the light curve shape is only slightly influenced by this parameter. We have verified that our results are independent of the exact value of K within this range and then adopted $K=0.001$.

It is possible to derive a relation between the surface temperature T_{surf} and the magnetic colatitude χ ($\chi = 0$ at the magnetic poles):

$$T_{surf}(\chi) = T_{eff} \left[1 - 0.47(1 - K) \right]^{-1/4} \left[\frac{K + (4 - K) \cos^2 \chi}{1 + 3 \cos^2 \chi} \right]^{1/4} \quad (1)$$

where T_{eff} is the effective temperature of the star, i.e. the temperature of the blackbody with the same bolometric luminosity of a source with a temperature distribution given by (1). In the following, we have estimated T_{eff} on the basis of the results of blackbody spectral fits. In fact, the spectra produced by (1) cannot be distinguished from that of a blackbody at T_{eff} within the limited energy resolution and statistics of the present observations. Due to the effects of the radiative transport in the neutron star atmosphere on the emerging spectra, the surface temperature can differ from that derived with pure blackbody fits (Romani 1987, Shibano et al. 1992). However, the exact value of T_{eff} adopted in the computations has little effect on the degree of modulation of the resulting light curves, which mainly depend on orientation and gravitational effects. Since our results would remain practically unchanged for any other locally isotropic emission spectrum, we have adopted for simplicity the blackbody model.

The magnetosphere of a neutron star is characterized by strong magnetic fields, high-energy photons and charged particles of opposite polarities. It is not surprising that, under favourable conditions, a fraction among the charged particles is accelerated towards the star (see, e.g. Arons 1981; Cheng, Ho & Ruderman 1986a, 1986b), colliding with it in the polar-cap regions. The kinetic energy of the impinging particles produces a reheating of the caps, which become hotter than the contiguous regions. To account for this phenomenon, we

introduce two hot areas near the magnetic poles: their temperature, T_{cap}^∞ , and angular size, θ_{cap} , are determined from the results relative to the hard tail.

This relatively simple model applies if the surface magnetic field is the primary factor in determining the temperature distribution: it becomes invalid if the thermal structure at the neutron star surface is instead controlled by irradiation of hard X-rays backscattered in the magnetosphere (Halpern & Ruderman 1993). Moreover, absorption and scattering of radiation in the magnetospheric plasma can alter the pulse profiles and weaken the effect of an anisotropic surface temperature distribution (Zavlin, Shibano & Pavlov 1995). These effects are not included.

Since the soft X-ray emission originates at the neutron star’s surface, where the gravitational field is very strong, the propagation of this radiation must be examined in the framework of general relativity. The two outstanding effects (Page 1995a) are the change of the energy of the photons along their path (gravitational red-shift) and the bending of their trajectories (gravitational bending). We include both effects in the calculation of the light curves and spectra, using the method outlined by Pechenick et al. (1983). The physical parameter describing the extent of the relativistic effects is $(1+z) = (1 - 2GM/Rc^2)^{-1/2}$.

After applying these corrections, the light curves are derived by integrating the contributions of all the surface elements visible at a given phase. The resulting emission is then folded through the interstellar absorption and the instrumental response.

The modulation of the light curves depends on the angles between the spin and magnetic axes (α) and between the latter and the line of sight (β). We have considered the values derived for PSR 0656+14 by radio observations. Two different approaches (Lyne & Manchester 1988; Rankin 1993) have been used to interpret the variety of pulse shapes, polarization patterns and spectra of radio pulsars. For several objects these models lead to significantly different results (see Miller & Hamilton 1993, for a comparison of the two methods). For PSR 0656+14, Lyne & Manchester derived $\alpha = \beta = 8.2^\circ$, while Rankin only gave an estimate for $\alpha = 30^\circ$, similar to the value ($\alpha = 35^\circ$) independently obtained by Malov (1990).

3.2 Results

Based on the above model and using the values of N_H , T_{eff}^∞ , T_{cap}^∞ , θ_{cap} obtained from the spectral fits of §2, we have simulated various light curves. T_{eff} and T_{cap} are fixed by choosing different values of $(1+z)$ and the corresponding light curves are compared to the observations.

If PSR 0656+14 is in the geometrical configuration proposed by Rankin ($\alpha = 30^\circ$), the calculated light curves can satisfactorily reproduce the observed degree of modulation only if $1.10 \leq (1+z) \leq 1.15$. Figure 4 compares the observed 0.1–2.4 keV light curve to that computed with the values of reference shown in the central column of Table 2, giving a pulsed fraction $P_{fr} = 7.5\%$. If $(1+z)$ is increased, P_{fr} reduces significantly and the resulting light curves are inconsistent with the observation. As shown in Table 2, P_{fr} is little affected by the values of the remaining parameters, except for β (which cannot be much larger than 10° otherwise the pulsar would not be visible in the radio band).

Table 2: Pulsed fractions of the simulated light curves (0.1–2.4 keV) as a function of the adopted parameters.

parameters		reference values	
N_H (cm^{-2})	$1.7 \cdot 10^{19}$	$6.86 \cdot 10^{19}$	$23 \cdot 10^{19}$
	7.06%	7.46%	8.35%
T_{eff}^∞ ($^\circ K$)	$0.50 \cdot 10^6$	$0.91 \cdot 10^6$	$1.30 \cdot 10^6$
	8.81%	7.46%	7.10%
K	0.0001	0.0012	0.01
	7.46%	7.46%	7.36%
θ_{cap}	0°	3.4°	
	7.00%	7.46%	
T_{cap}^∞ ($^\circ K$)	$1.50 \cdot 10^6$	$1.90 \cdot 10^6$	$2.30 \cdot 10^6$
	7.30%	7.46%	7.76%
β	-10°	0°	$+10^\circ$
	5.56%	7.46%	7.65%
$1 + z$	1.10	1.15	1.20
	9.87%	7.46%	5.15%
α	8.2°	30.0°	35.0°
	<i>L.&M.</i>	<i>Rankin</i>	<i>Malov</i>
	1.46%	7.46%	8.55%

The adopted parameters of reference are shown in the central column. Next to them, we report a set of values spanning the reliable range of variability for each quantity. The pulsed fractions indicated below each number are those obtained by setting all the other parameters at the reference values. The observed pulsed fraction is in the range [8–10%].

The emission from the polar caps gives only a modest increase to the pulsed fraction in the 0.1 – 2.4 keV range, dominated by the contribution of the softer blackbody.

Following the same procedure, we have computed the light curves for the angles suggested by Lyne & Manchester ($\alpha = 8.2^\circ$, $\beta = 8.2^\circ$). Our model cannot explain the relatively high observed modulation, even for the unacceptable value of $(1 + z) = 1.00$. Using the combination of parameters which maximizes the modulation, the predicted P_{fr} would reach at most 4%, much less than the minimum value compatible with the observations. Thus, as also indicated by Page (1995a), the small dipole inclination angle proposed by Lyne & Manchester (1988) cannot account for the observed pulsed fraction (see also Possenti, Mereghetti & Colpi 1996).

4 Conclusions

The ROSAT spectral and timing analysis of PSR 0656+14 indicate that its soft X-ray emission is characterized by two separate components. The blackbody

temperature of the softer component (9×10^5 °K), independent of the model used for the hard tail, is similar to that derived by Finley et al. (1992).

The hard tail can be described equally well by a blackbody or by a steep power law. In the blackbody case, it is natural to attribute the hard component to localized emission from hotter regions of the star surface, e.g. the polar caps, as discussed above. In the case of a power law, the tail can be interpreted as a non-thermal emission of magnetospheric origin. The best fit power law index ($\Gamma = 4.5$) is greater than that observed in PSR 1055–52 ($\Gamma = 1.5$, Ögelman & Finley 1993) and Geminga ($\Gamma = 2.5$, Halpern & Ruderman 1993), the other isolated neutron stars of comparable age and with a similar two component soft X–ray emission. These two objects have also been clearly observed at γ -ray energies ($E \gtrsim 100$ MeV), contrary to PSR 0656+14 for which only a marginal detection, at a much lower flux, has been claimed (Ramanamurthy et al. 1996). This fact might indicate a possible connection between the level of γ -ray emission and the slope of the hard X–ray tail.

With a model for the anisotropic thermal cooling induced by the crustal, dipolar magnetic field (similar to our first component), Page (1995a) derived for PSR 0656+14 pulsed fractions between 8 and 10%, smaller than that ($\simeq 14\%$) reported by Finley et al. (1992). This result is confirmed by our analysis of the complete PSPC data set. We show that, even in the most favourable geometric configuration ($\alpha \sim 30^\circ$) among those compatible with the radio data, the observed modulation can be reproduced only for $(1+z) \leq 1.15$ (corresponding to $R/R_S \gtrsim 4$, where R_S is the Schwarzschild radius). These low values of z are consistent with a stellar radius between 12 and 17 km and a neutron star mass $M \sim 1M_\odot$. For $M = 1.4 M_\odot$, our limit on z requires a radius ~ 17 km, a value inconsistent with the most recent neutron star models (Glendenning 1985; Wiringa et al. 1988). Masses below $1.4 M_\odot$ have radii sufficiently large to account for the observed modulation in the X-ray signal, only if the equation of state is very stiff (Page 1995a).

The presence of higher order moments in the magnetic field, or the effects of a magnetized atmosphere causing anisotropic photon transport have been proposed as solutions for increasing the light curve modulation (Page 1995a, 1995b). Our analysis shows that the alternative possibility of obtaining a higher modulation by including the additional contribution of hot polar caps does not solve the problem. The polar cap emission has little effect on the overall modulation, if its temperature and intensity are to be consistent with the observed spectra.

References

- [–] Arons J., 1981, *Pulsars*, IAU Symp. 95, eds W.Sieber, R. Wielebinski (Dordrecht: Reidel), 69
- [–] Caraveo P., Bignami G.F. & Mereghetti S., 1994, *ApJ*, 422, L87
- [–] Cheng K.S., Ho C. & Ruderman M., 1986a, *ApJ*, 300, 500
- [–] Cheng K.S., Ho C. & Ruderman M., 1986b, *ApJ*, 300, 522

- [-] Cordova F.A. et al., 1989, ApJ, 345, 451
- [-] Finley J.P., Ögelman H. & Kiziloğlu Ü., 1992, ApJ, 394, L21
- [-] Glendenning N.K., 1985, ApJ, 293, 470
- [-] Greenstein G. & Hartke G.J., 1983, ApJ, 271, 283
- [-] Halpern J.P. & Ruderman M., 1993, ApJ, 415, 286
- [-] Hernquist L., 1985, MNRAS, 213, 313
- [-] Lyne A.G. & Manchester R.N., 1988, MNRAS, 234, 477
- [-] Malov I.F., 1990, Astron. Zh., 67, 377 (Sov. Astron. 34, 189)
- [-] Miller C.M. & Hamilton R.J., 1993, ApJ, 411, 298
- [-] Nousek J.A. et al., 1981, ApJ, 248, 152
- [-] Ögelman H., 1995, in *Lives of the Neutron Stars*, ed. A.Alpar, Ü. Kiziloğlu & J. van Paradijs (Dordrecht: Kluwer), 101
- [-] Page D., 1995a, ApJ, 442, 273
- [-] Page D., 1995b, Sp.Sc.Rev., in press
- [-] Page D., Shibanov Yu.A. & Zavlin V.E., 1995, ApJ, 451, L21
- [-] Pechenick K.R., Ftaclas C. & Cohen J.M., 1983, ApJ, 274, 846
- [-] Possenti A., Mereghetti S. & Colpi M., 1996, Proc. of *Röntgenstrahlung from the universe*, Würzburg, in press
- [-] Ramanamurthy P.V. et al., 1996, ApJ, 458, 755
- [-] Rankin J., 1993, ApJ, 405, 285
- [-] Romani R.W., 1987, ApJ, 313, 718
- [-] Schaaf M.E., 1990, A&A, 227, 61
- [-] Taylor J.M., Manchester R.N., Lyne A.G. & Camilo F., 1995, ftp:pulsar.princeton.edu
- [-] Thompson R.J.Jr. & Cordova F.A., 1994, ApJ, 421, L13
- [-] Thompson R.J.Jr. et al., 1991, ApJ, 366, L83
- [-] Shibanov Yu. et al., 1992, *Isolated Pulsars*, Cambridge University Press, 160
- [-] Wirling R.B., Fiks V. & Fabrocini A., 1988, Phys. Rev., C38, 1010
- [-] Zavlin V.E., Shibanov Yu.A. & Pavlov G.G., 1995, Astron. Lett., 21, 149

Captions

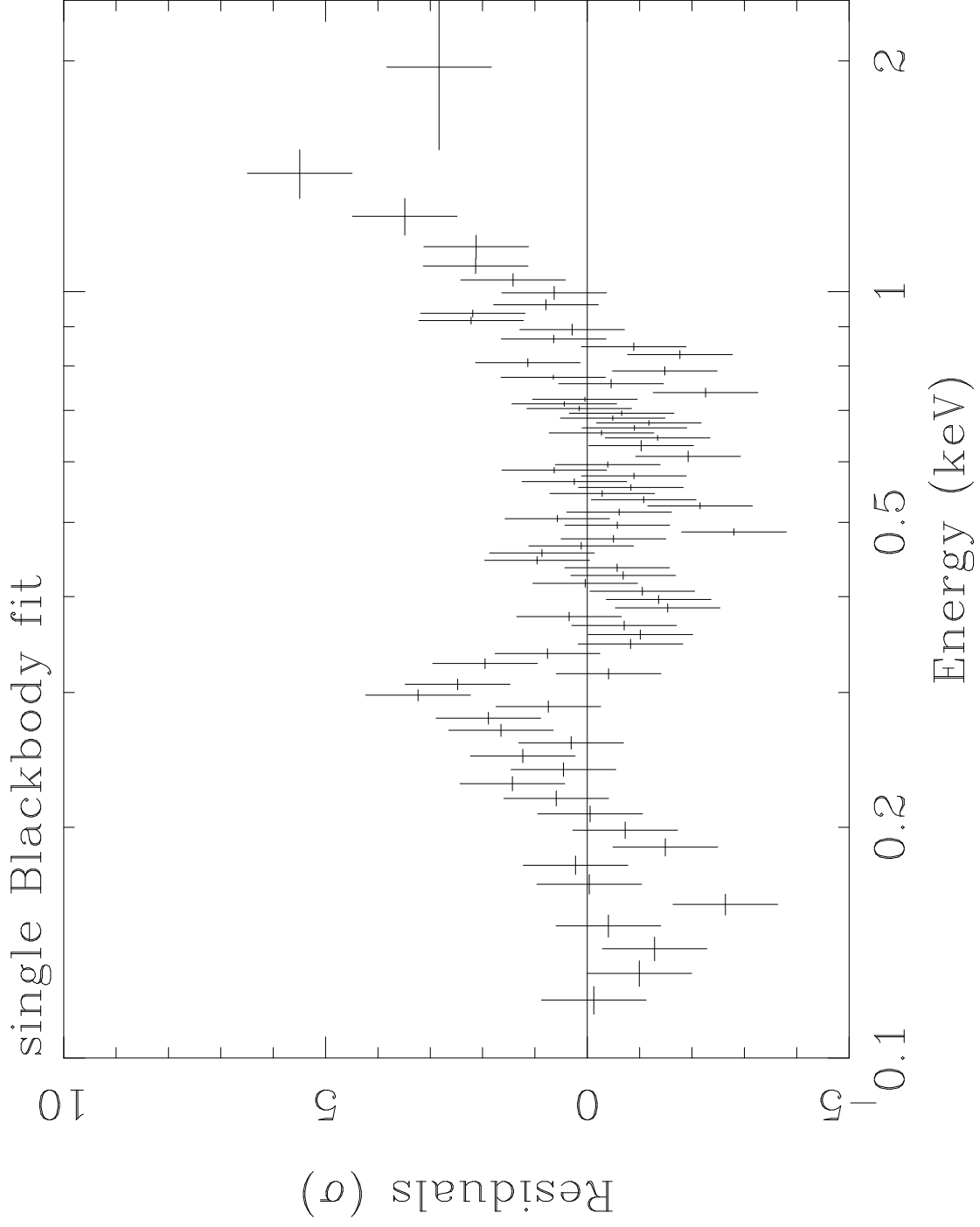
Figure 1: Residuals of the best fit with a single blackbody ($T^\infty = 1.0 \times 10^6$ °K, $N_H = 5 \times 10^{19}$ cm $^{-2}$, $\chi^2 = 2.20$ for 76 dof). The presence of a hard tail above 1 keV is clearly visible.

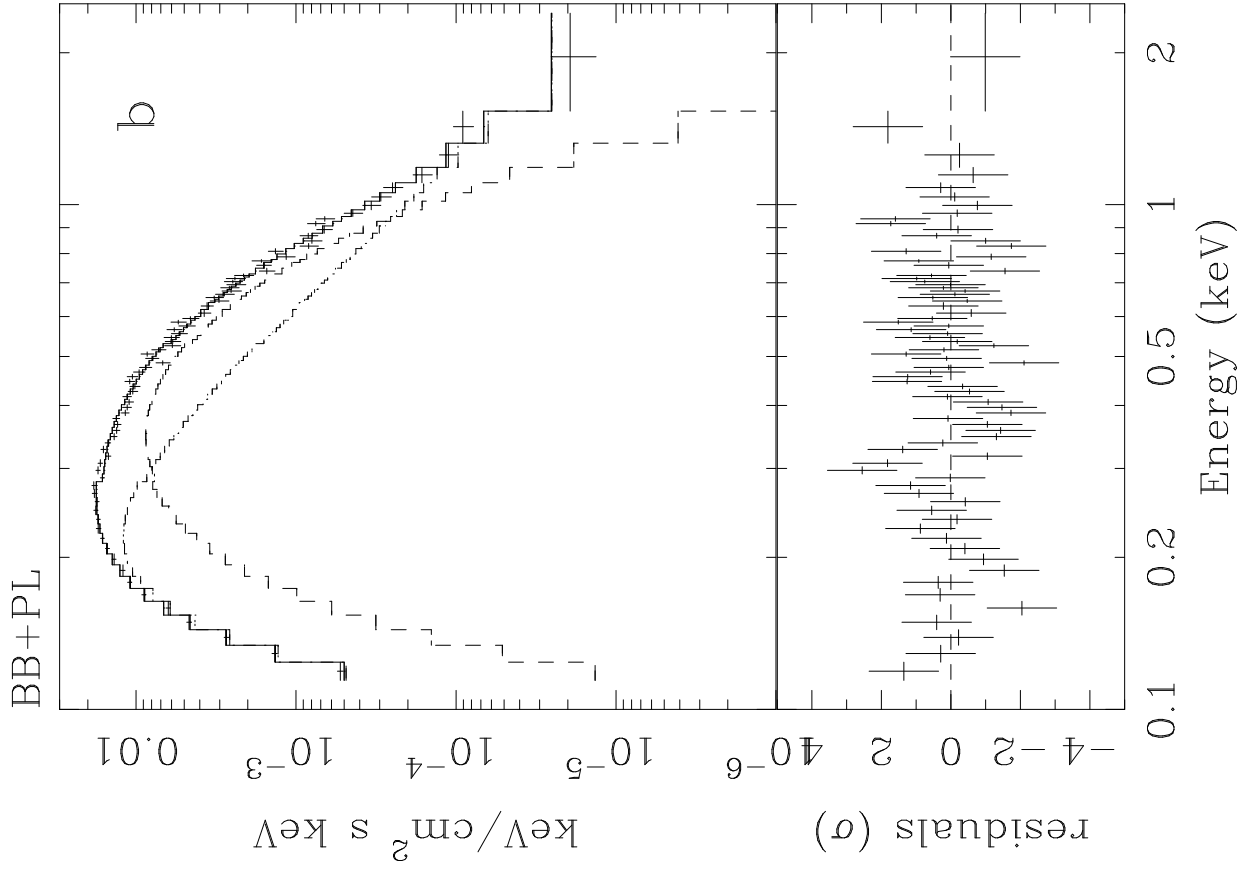
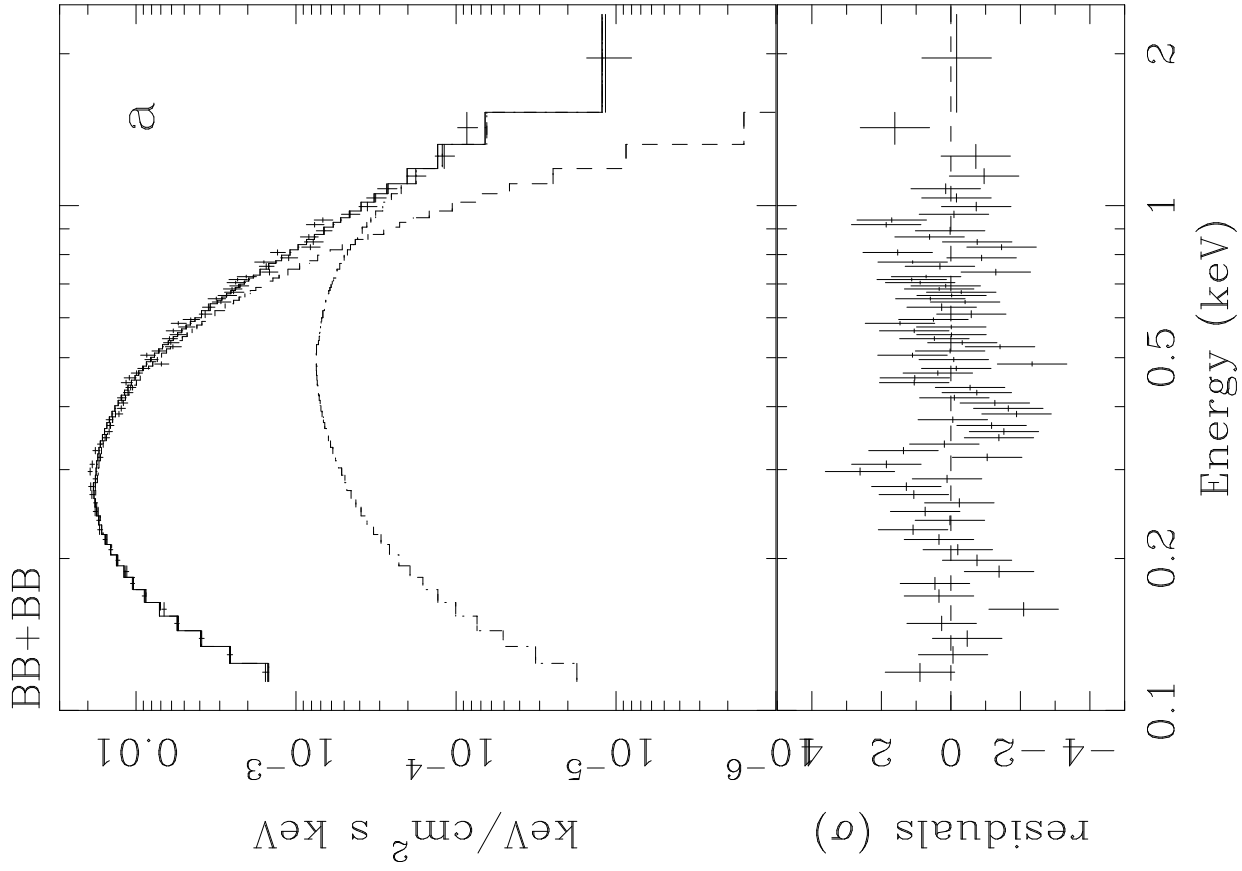
Figure 2: Results of the fits with two component models: **(a)** two blackbody components; **(b)** sum of a blackbody and a power law.

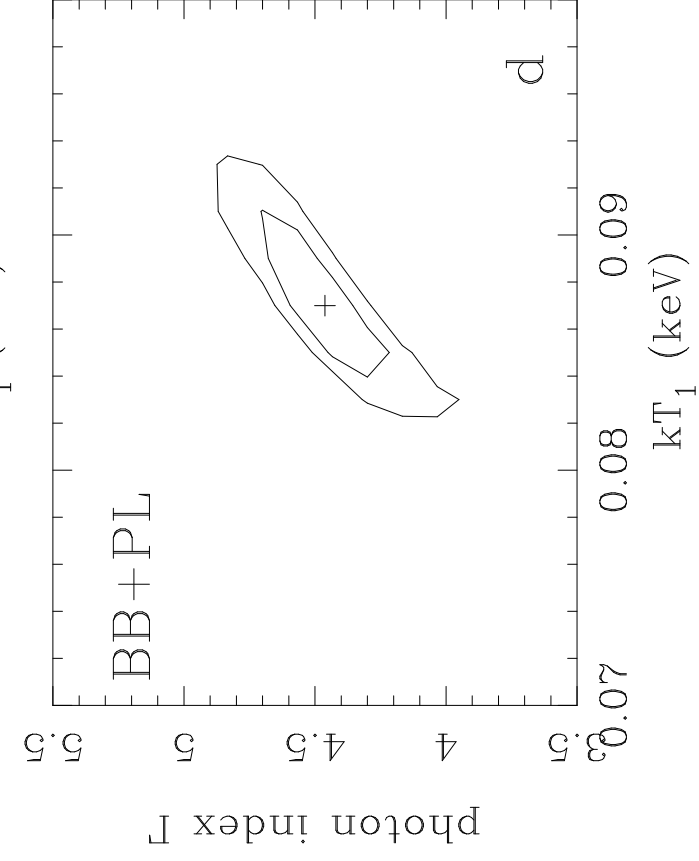
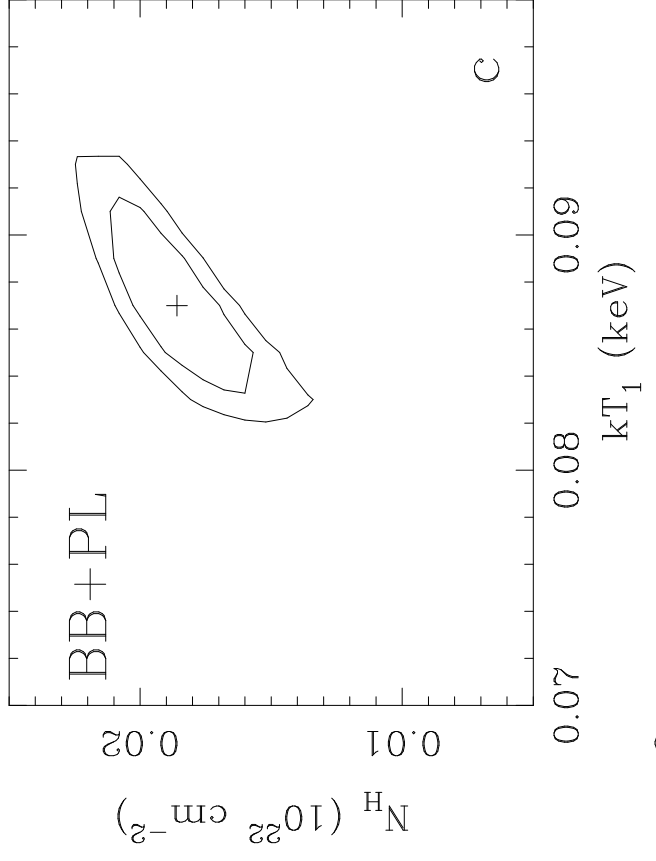
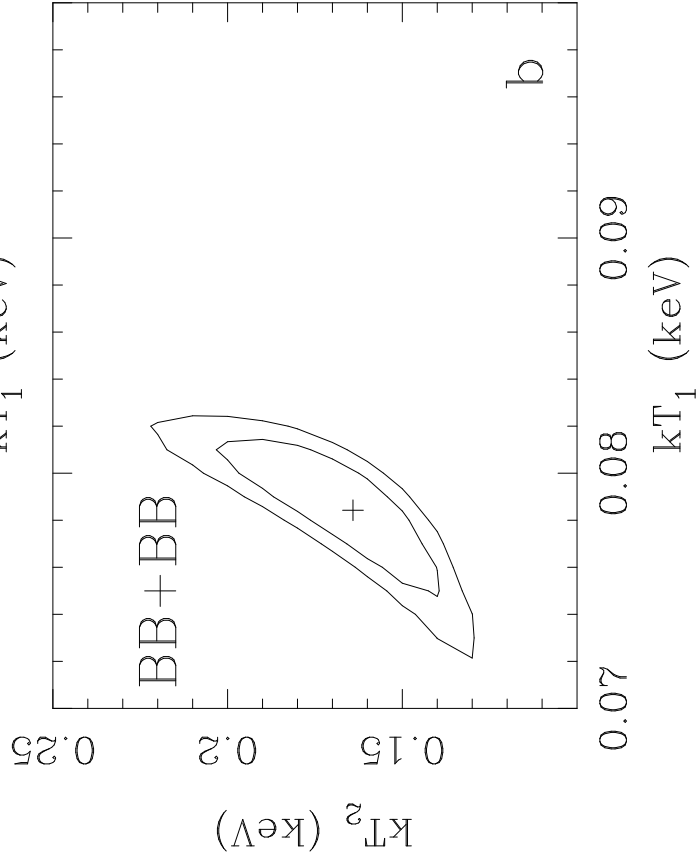
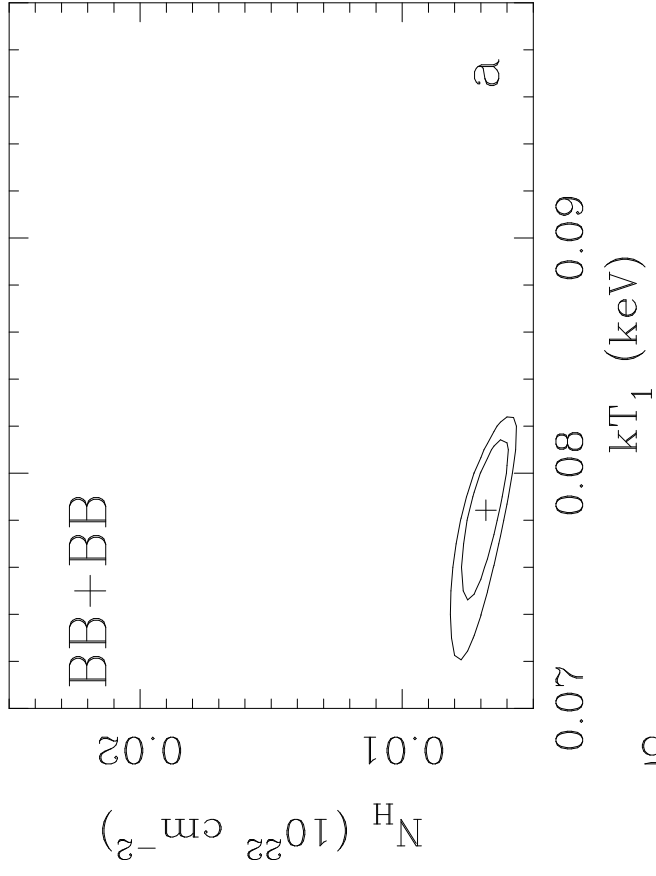
Figure 3: Confidence contours (68% and 90% confidence level) for two interesting parameters. **(a)** and **(b)** refer to the fit with two blackbodies; **(c)** and **(d)** to the blackbody plus power law case.

Figure 4: Comparison between the PSPC light curve of PSR 0656+14 in the energy range [0.10–2.40] keV (solid line) and that calculated with the reference parameters of Table 2 (dotted line). A typical error bar is shown.

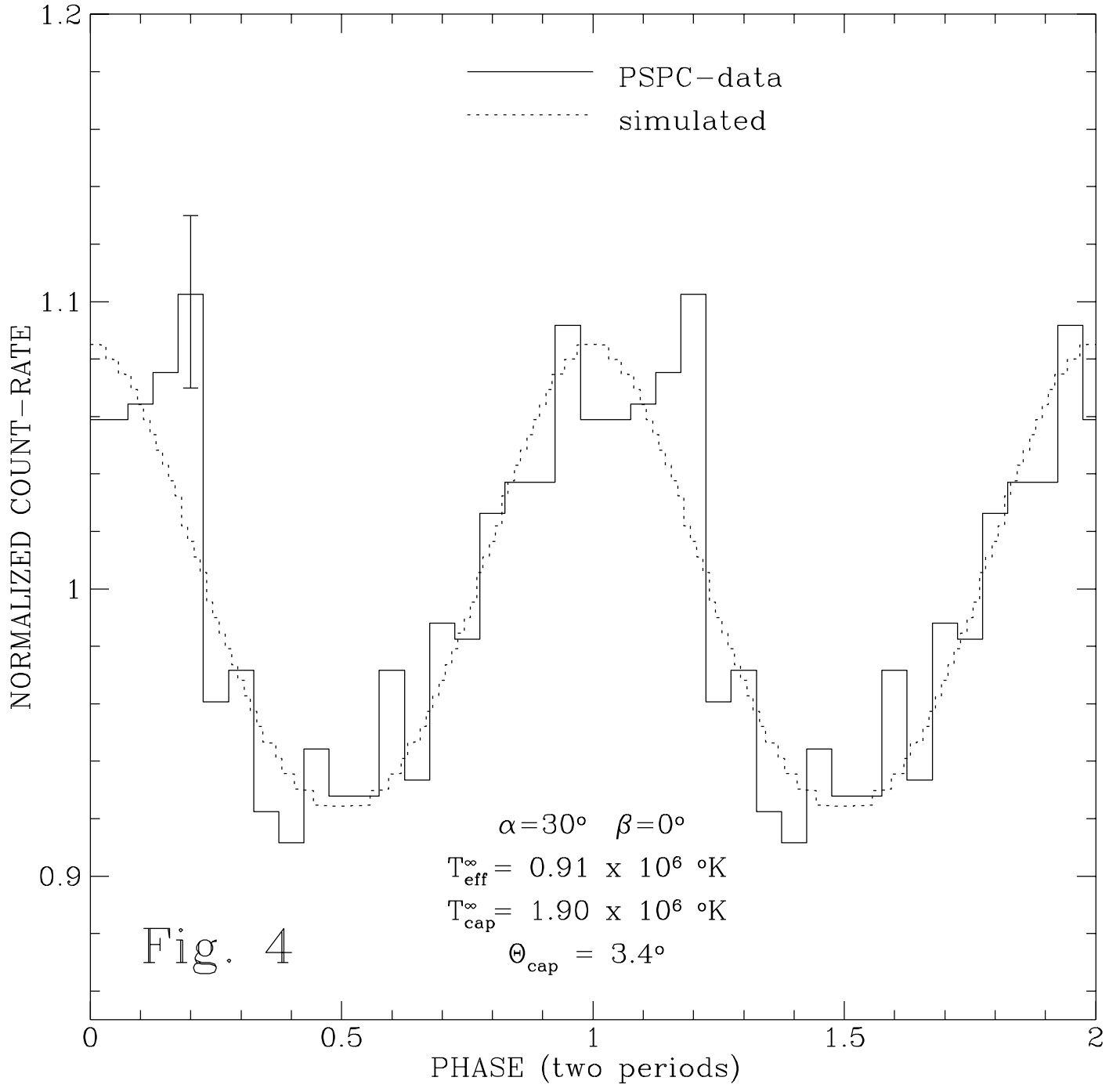
Figure 5: Background subtracted light curves of PSR 0656+14 in three different energy ranges. From top to bottom: 0.10–0.24 keV, 0.24–0.55 keV and 0.55–2.40 keV. Each curve has been normalized dividing by the average number of counts per phase bin (respectively: 582, 579, 94 counts in the low, medium and high energy range). The light curves have been smoothed with a running average algorithm with five bins width.



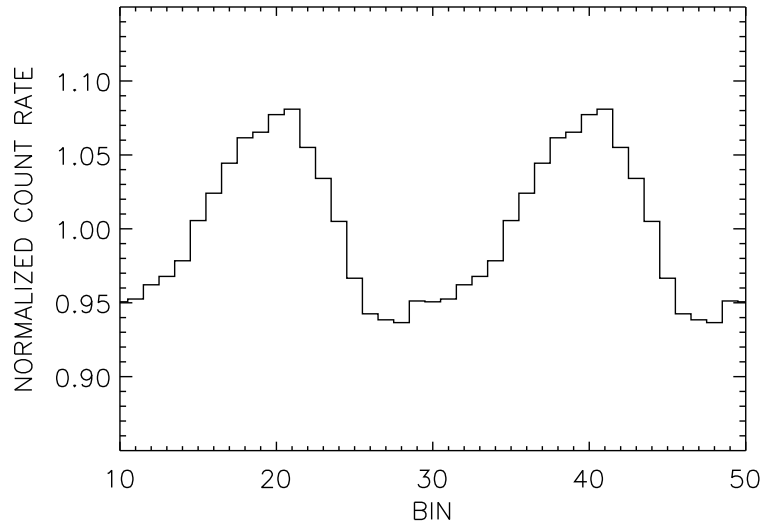




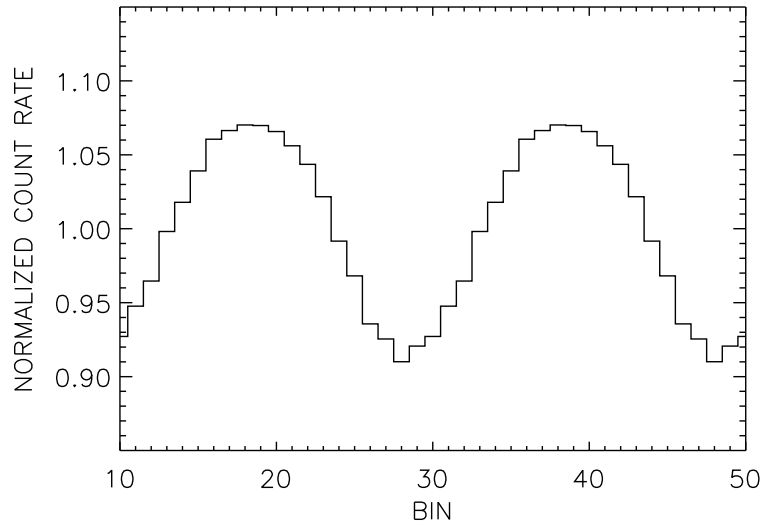
PSR0656+14 [0.10 : 2.40] KeV



0.1–0.24 keV



0.24–0.55 keV



0.55–2.4 keV

